DOI: 10.53469/wjimt.2024.07(05).16

Multi-Beam Surveying Ocean Exploration Model and Applications

Wenbo Yang*, Zhenzhen Li, Fei Tang

Jiamusi University, School of Mechanical Engineering, Jiamusi 154007, China
Correspondence Author, 2051704436@qq.com

Abstract: ***With the development of artificial intelligence, fiber Bragg grating (FBG) sensing technology has garnered increasing attention. This paper first proposes a surface reconstruction algorithm based on curvature information, which is applicable to two different sensor structures: implanted FBG sensors and whisker array sensors. The design and analysis of these sensors are based on a pure bending model, where the corresponding bending curvature is obtained by measuring the wavelength shift of the fiber Bragg grating at the measurement points. Next, the paper elaborates on the surface reconstruction algorithm for the implanted FBG sensor. This sensor contains FBG sensing points that are evenly distributed. Curvature information corresponding to the position can be obtained based on the direction and magnitude of the wavelength shift. The fiber bending is considered as a connection of multiple arc segments, and the coordinates of the sensing points are calculated in the Cartesian coordinate system using the properties of the tangents. The fiber bending curve is then reconstructed by connecting the arc segments in MATLAB. Finally, the paper provides a detailed introduction to the surface reconstruction algorithm for the whisker array sensor. When the whiskers bend, the FBGs fixed on them act as curvature sensors. The curvature is determined by the FBG wavelength shift, and the three-dimensional coordinates of the whisker tip relative to the base are calculated based on a geometric model. MATLAB is then used to connect the whisker tip coordinates, completing the construction of the surface.***

Keywords: Fiber Bragg Grating Sensing Technology; Surface Reconstruction Algorithm; Implanted *FBG* Sensor; Whisker Array Sensor.

1. INTRODUCTION

With the development of artificial intelligence, the demand for tactile sensors in intelligent robots is increasingly growing. Fiber Bragg Grating (*FBG*) is a type of optical structure with periodic refractive index modulation. This sensor detects changes in the external environment by monitoring variations in the Bragg wavelength. It has several unique advantages, such as high sensitivity, immunity to electromagnetic interference, good corrosion resistance, small size, light weight, and the capability for multi-point distributed measurements, making it a highly promising optical sensing technology applicable to various fields. There are two different types of *FBG* sensors: the embedded *FBG* sensor and the whisker-array *FBG* sensor. The embedded *FBG* sensor measures the curvature information by detecting the sensing points, reconstructs the fiber bending curve using a geometric model, and subsequently constructs the surface. On the other hand, the whisker-array *FBG* sensor measures the bending curvature at the *FBG* sensing points on the whiskers, calculates the three-dimensional coordinates of the whisker tips relative to the base during bending, and ultimately reconstructs the surface. Both surface reconstruction algorithms are based on a pure bending model, where the bending curvature is obtained by measuring the wavelength shift of the fiber Bragg grating. These algorithms involve minimal computational complexity and are based on simple and understandable principles, laying the foundation for the sensor's ability to construct the shape and surface of objects.

Venketeswaran [1] et al. proposed that optical fiber sensing technology, characterized by long-distance, high-precision, and distributed measurement, can overcome its shortcomings such as cross-sensitivity and low data processing speed when combined with machine learning and artificial intelligence. Floris [2] et al. stated that optical fiber shape sensing is an innovative technology that continuously tracks the 3D shape and position of dynamic objects without visual contact using fiber optic cables. Lu [3] et al. proposed a novel 3D shape sensing algorithm that incorporates a universal model filtering technique and an enhanced moving average method. They utilized *FBG* sensors to improve shape sensing and position estimation accuracy in flexible endoscopic surgeries. Liu [4] et al. introduced a multifunctional sensor based on a triangular four-core fiber with a helical twist structure assisting a fiber Bragg grating. This sensor measures directional twist and vector bending while eliminating the effects of temperature and strain through the design of the helical twist region. Lefloch [5] et al. introduced curvature information and proposed a real-time scene reconstruction method based on surface curvature, which reduces error accumulation caused by drift in the *ICP* algorithm. Le Tien [6] et al. proposed a sparsity algorithm

based on octree subdivision, using curvature grouping to analyze and recognize the surfaces of 3D objects. Ferraro [7] et al. showed that a causal algorithm based on dynamic thresholds combined with hybrid convolutional and recurrent neural networks can be used with sensors to monitor heart activity. Sefati [8] et al. embedded a fiber Bragg grating array and Nitinol wires within a three-chamber polycarbonate tube, making the large deflection FBG sensor more robust, repeatable, and cost-effective, enabling high-precision curvature detection. Mohapatra [9] et al. proposed the use of finite element analysis to design fully encapsulated fiber Bragg grating sensors for cardiovascular feature acquisition. Ngiejungbwen [10] et al. provided a comprehensive analysis of the use of sensors such as fiber Bragg grating sensors in healthcare and remote sensing applications. Ramly [11] et al. introduced an intelligent material for aircraft structures that embeds fiber Bragg grating sensors within carbon fiber sandwich panels, enabling real-time and high-precision structural health monitoring. Kent [12] et al. proposed a camera-based whisker array sensing system that measures the relative motion between each whisker and the skin and developed an algorithm to differentiate between inertial forces and airflow. Yang Haokun [13] et al. designed and validated a sensor based on a fiber Bragg grating whisker array, which reconstructs the surface of an object with high precision by analyzing the wavelength shifts and bending curvature of the fiber Bragg gratings. Kent [14] et al. proposed a novel whisker sensing system that uses tapered flexible whiskers to provide tactile sensing input, combined with a gradient moment algorithm and torque algorithm to improve the accuracy of radial contact distance estimation. Liang Wei [15] et al. combined fiber Bragg grating technology with a wet chemical etching process to study and propose two types of refractive index sensors: an etched single-mode fiber *FBG* and an etched fiber Fabry-Perot interferometer (*FFPI*). Both sensors can be used as point sensors for measuring liquid refractive index and concentration changes.

Based on the previous research status and problem background, the main work of this paper is to propose and elaborate on two surface reconstruction algorithms based on a pure bending model. These are the surface reconstruction algorithm based on embedded FBG-type sensors and the surface reconstruction algorithm based on whisker array-type sensors.

2. ALGORITHM FOR SURFACE RECONSTRUCTION BASED ON CURVATURE

Based on the structural characteristics of the sensors, the surface reconstruction method for the implanted FBG-type sensor utilizes the curvature information obtained from the implanted *FBG* sensing points. Through geometric models and theoretical curve reconstruction, these reconstructed curves are further used to build the surface. For the surface reconstruction method used with the whisker array sensor, the curvature information is obtained from the *FBG* sensing points on each whisker, and the distance from the tip of each whisker to the base is calculated using geometric theory to determine the coordinate information of the whisker tip. This coordinate information is then used to reconstruct the surface.

The design and analysis of the implanted FBG-type sensors and whisker array sensors are based on a pure bending model. Under the condition of pure bending deformation, the formula for calculating the wavelength shift of the fiber Bragg grating at the measurement point for a fiber micro-element with thickness d and length L is given by Equation (1).

$$\Delta\lambda_B = \frac{k(1-P_e)d\lambda_B}{2} \tag{1}$$

The parameters P_e, d and λ_B are all constants. According to Equation (1), the wavelength shift $\triangle\lambda_B$ has a linear relationship with the bending curvature k. Therefore, to calculate the bending curvature information, one can measure the wavelength shift data of the fiber Bragg grating at the measurement point.

3. SURFACE RECONSTRUCTION ALGORITHM WITH EMBEDDED FBG SENSORS

In this surface reconstruction algorithm, the *FBG* (Fiber Bragg Grating) sensors are embedded by inserting a fiber optic cable with multiple uniformly distributed *FBGs* into a thin silicone sheet at a specific depth. When this sensor is adhered to the surface of an object, this paper assumes that each fiber optic cable has 3 *FBG* sensing points. The bending of each fiber can be summarized into two cases as shown in Figures 1 and 2, which can be determined based on the direction of the *FBG* wavelength shift. By analyzing the wavelength shifts at the *FBG* measurement points, curvature information at corresponding positions can be obtained, which can then be used to reconstruct the bending curve of the fiber optic cable. Assuming that each fiber optic cable has 3 uniformly distributed *FBG* sensing points, when the fiber bends, it can be regarded as consisting of 3 arc segments, denoted as *AB*, *BC*, and

CD. By using the curvature information of these 3 arc segments, the equations for each arc segment can be determined, and connecting these segments will reveal the overall bending condition of the fiber optic cable. The overall bending condition of the fiber optic cable can be categorized into two cases when connecting the 3 arc segments, with the first case illustrated in Figure 1.

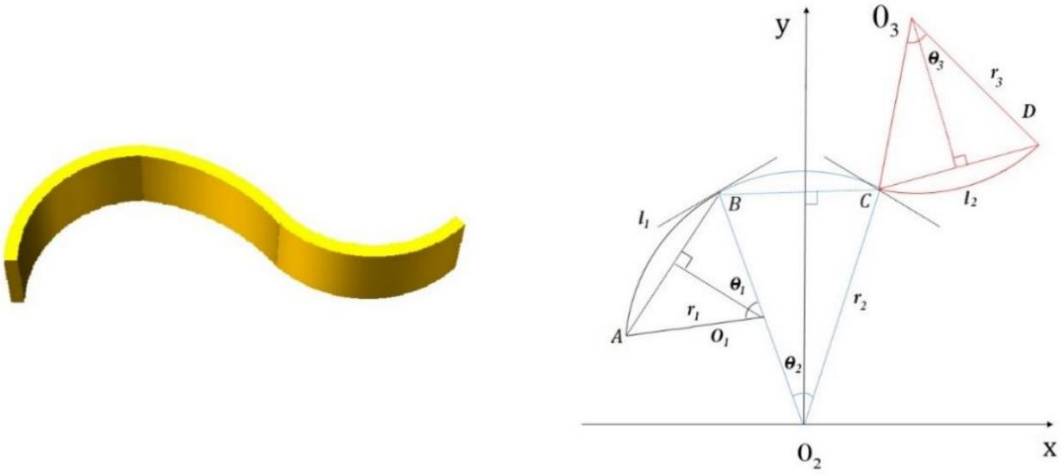

Figure 1: Flexible Sensor and Fiber Bending: First Case

As shown in Figure 1, line l_1 is the common tangent to arc segments *AB* and *BC*, and line l_2 is the common tangent to arc segments *BC* and *CD*. Thus, the tangent at the boundary between two adjacent arc segments is the same. Therefore, in the Cartesian coordinate system, the coordinates of all sensor points can be calculated.

Assuming the coordinates of the centers of the three arcs are $O_1(x_1, y_1)$, $O_2(0, 0)$, and $O_3(x_3, y_3)$, with corresponding radii of curvature r_1, r_2 and r_3 respectively. In the coordinate system, the coordinates of O_1 are as given by formula (2).

$$\begin{cases} x_1 = -(r_2 - r_1)\sin\frac{\theta_2}{2} \\ y_1 = (r_2 - r_1)\cos\frac{\theta_2}{2} \end{cases} \tag{2}$$

Among them, x_1 is the x-coordinate of the center O_1 of the arc segment *AB*, y_1 is the y-coordinate of the center O_1 of the arc segment *AB*, r_1 is the radius of curvature for the arc segment *AB*, and r_2 is the radius of curvature for the arc segment *BC*.

The coordinates of O_3 are as shown in formula (3).

$$\begin{cases} x_3 = (r_2 + r_1)\sin\frac{\theta_2}{2} \\ y_3 = (r_2 + r_1)\cos\frac{\theta_2}{2} \end{cases} \tag{3}$$

In this context, x_3 is the x-coordinate of the center O_3 of the circular arc segment *CD*, y_3 is the y-coordinate of the center O_3 of the circular arc segment *CD*, r_1 is the radius of curvature for the arc segment *AB*, and r_2 is the radius of curvature for the arc segment *BC*.

The coordinates of the arc endpoint *A* are given by formula (4).

$$\begin{cases} x_A = -[2r_1\sin\frac{\theta_1}{2}\cos(\frac{\theta_1}{2} + \frac{\theta_2}{2}) + r_2\sin\frac{\theta_2}{2}] \\ y_A = r_2\cos\frac{\theta_2}{2} - 2r_1\sin\frac{\theta_1}{2}\cos(\frac{\theta_1}{2} + \frac{\theta_2}{2}) \end{cases} \tag{4}$$

Here, x_A and y_A represent the coordinates of arc endpoint *A* on the x-axis and y-axis, respectively. r_1 is the radius of curvature corresponding to arc segment *AB*, and r_2 is the radius of curvature corresponding to arc segment *BC*.

The coordinates of arc endpoint *B* are shown in Equation (5).

$$\begin{cases} x_B = -r_2 \sin\frac{\theta_2}{2} \\ y_B = r_2 \cos\frac{\theta_2}{2} \end{cases} \tag{5}$$

The coordinates x_B and y_B represent the x-axis and y-axis coordinates of arc endpoint B, respectively, while r_2 is the radius of curvature corresponding to arc segment BC.

The coordinates of arc endpoint C are shown in equation (6).

$$\begin{cases} x_C = r_2 \sin\frac{\theta_2}{2} \\ y_C = r_2 \cos\frac{\theta_2}{2} \end{cases} \tag{6}$$

Here, x_C and y_C represent the x-axis and y-axis coordinates of arc endpoint C, respectively. r_2 is the radius of curvature corresponding to arc segment BC.

The coordinates of arc endpoint D are shown in Equation (7).

$$\begin{cases} x_D = r_2 \sin\frac{\theta_2}{2} + 2r_3 \sin\frac{\theta_3}{2}\cos\left(\frac{\theta_3}{2} + \frac{\theta_2}{2}\right) \\ y_D = r_2 \cos\frac{\theta_2}{2} + 2r_3 \sin\frac{\theta_3}{2}\cos\left(\frac{\theta_3}{2} - \frac{\theta_2}{2}\right) \end{cases} \tag{7}$$

In this context, x_D and y_D represent the x-axis and y-axis coordinates of the arc endpoint D, respectively. r_3 is the radius of curvature corresponding to arc segment CD, and r_2 is the radius of curvature corresponding to arc segment BC.

Therefore, the equation of arc AB is shown in equation (8).

$$[x + (r_2 - r_1)\sin\frac{\theta_2}{2}]^2 + [y + (r_2 - r_1)\cos\frac{\theta_2}{2}]^2 = r_1^2 \tag{8}$$

Among them, r_1 is the radius of curvature corresponding to arc segment AB, and r_2 is the radius of curvature corresponding to arc segment BC.

Then, the equation of arc BC is shown in equation (9).

$$x^2 + y^2 = r_2^2 \tag{9}$$

Here, r_2 is the radius of curvature corresponding to arc segment BC.

Then, the equation of arc CD is shown in equation (10).

$$[x - (r_2 + r_1)\sin\frac{\theta_2}{2}]^2 + [y - (r_2 + r_1)\cos\frac{\theta_2}{2}]^2 = r_3^2 \tag{10}$$

Among them, r_1 is the bending radius corresponding to arc AB, r_2 is the bending radius corresponding to arc BC, and r_3 is the bending radius corresponding to arc CD.

Using equations (8), (9), and (10), the arcs AB, BC, and CD can be connected with MATLAB to obtain the bending curve of the entire optical fiber. By connecting different bending curves, the shape of the object can be further obtained.

The second case is shown in Figure 2.

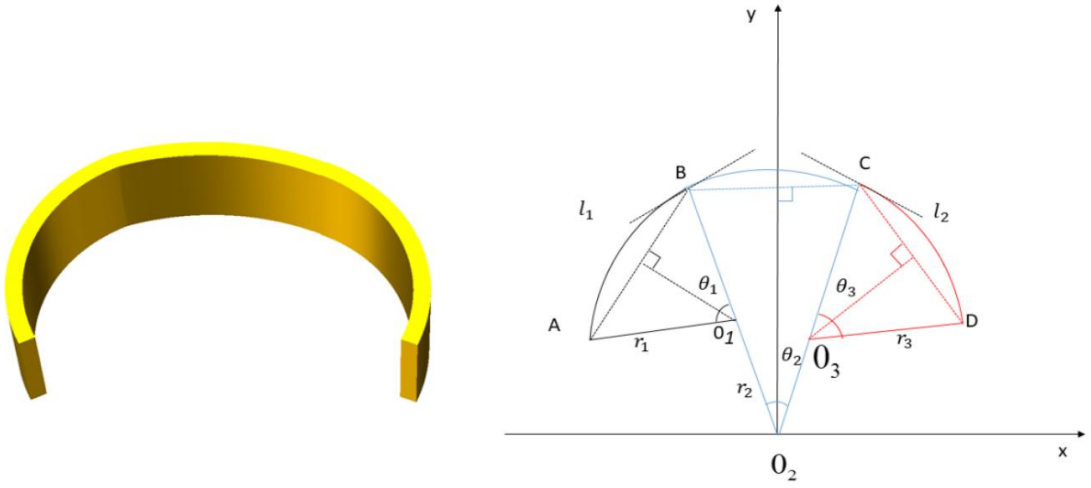

Figure 2: Flexible Sensor and Fiber Bending: Second Case

As shown in Figure 2, line l_1 is the common tangent to arc segments *AB* and *BC*, while line l_2 is the common tangent to arc segments *BC* and *CD*. This means that the tangent at the junction of two adjacent arc segments is the same. Therefore, in the Cartesian coordinate system, the coordinates of all sensing points can be calculated.

In this case, the coordinates of the circle centers, the coordinates of the arc endpoints, and the equations corresponding to the arcs can be derived in the same way as in the first scenario.

4. SURFACE RECONSTRUCTION ALGORITHM FOR WHISKER ARRAY SENSORS

When the whisker comes into contact with an object and bends, since the *FBG* is very thin and attached to the whisker, the *FBG* and the whisker can be considered as a uniform body under the same bending conditions. The Fiber Bragg Grating (*FBG*) attached to the whisker deforms along with the bending of the whisker, as shown in Figure 3.

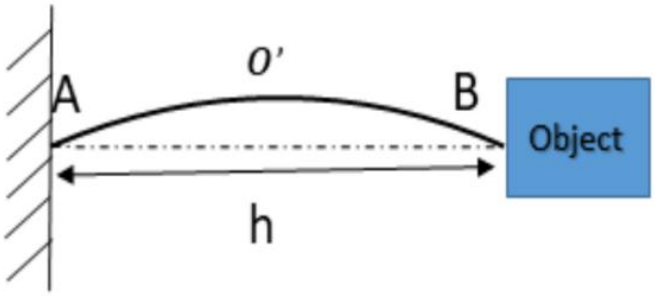

Figure 3: Mechanical properties of whiskers

As shown in Figure 3, *h* represents the straight-line distance between the endpoints *A* and *B* of the whisker, and *O*' is the midpoint of the whisker, which is also the fixed position of the fiber Bragg grating (*FBG*). Each sensing point *FBG* at the *O*' position can be considered as a curvature sensor, and the bending curve of each whisker can be regarded as an arc with a certain curvature.

Therefore, the whisker bending scenario can be viewed as a geometric model, as illustrated in Figure 4.

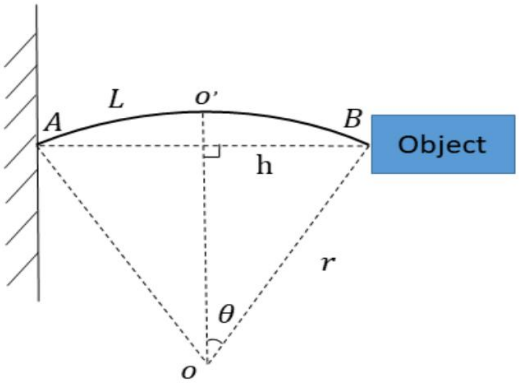

Figure 4: Geometric model of whiskers

As shown in Figure 4, h is the straight-line distance between the ends of the whisker, A and B; L is the length of the whisker between the ends A and B; O' is the midpoint of the whisker; A and B are the endpoints of the whisker; O is the center of the circle corresponding to the curved portion of the whisker; and r is the radius of the circle corresponding to the curved portion of the whisker. From this geometric model, formulas (11), (12), and (13) can be derived.

$$h = 2r \sin\theta \tag{11}$$

$$\theta = \frac{L}{r} \tag{12}$$

$$h = 2r \sin\left(\frac{L}{r}\right) \tag{13}$$

In this context, h represents the distance between the tip and the base of the whisker after the whisker bends upon contacting the object being measured. L is the initial length of the whisker, which is the length of arc AB. The curvature of the whisker can be calculated from the wavelength shift of the fiber grating. Therefore, the vertical distance h between the tip and the base of the whisker after contact with the object can be determined using equation (13).

As shown in Figure 5(a), a three-dimensional coordinate system is established where the base is defined as the x-axis and y-axis, and the whisker perpendicular to the base is defined as the z-axis. The x and y coordinates of the base of the whisker are known. Special measures are taken at the tip of the whisker to prevent it from sliding during bending when contacting the object. Additionally, it is ensured that the sensor remains perpendicular and without relative sliding with respect to the object during measurement. Consequently, the x and y coordinates of the tip of the whisker are the same as those of the base. As illustrated in Figure 5(b), the height h from the tip to the base of the whisker represents its coordinate along the z-axis, while the x and y coordinates remain unchanged. This allows for the determination of the three-dimensional coordinates of the whisker tip after bending upon contact with the object. Finally, the three-dimensional coordinates of the tips of all whiskers after contacting the object are calculated. MATLAB software is then used to connect the coordinates of all whisker tips to construct a surface model, which in turn reveals the shape of the surface of the object being measured.

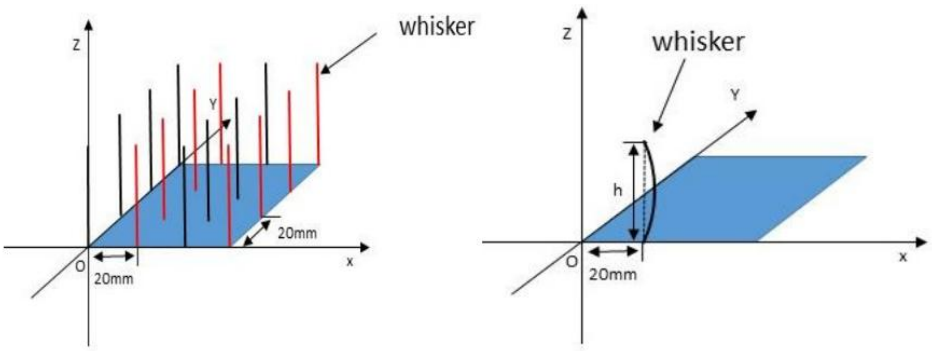

（a） (b)

Figure 5: Schematic Diagram of Whisker Array in Rectangular Coordinate System

5. SUMMARY

This paper mainly introduces curve and surface reconstruction algorithms used for sensor shape reconstruction. The algorithms are based on the curvature measurement principle of *FBGs*. Combining the FBG-based sensors and the whisker array-type sensors proposed in this paper, corresponding curve and surface reconstruction algorithms are provided. Both algorithms have the advantages of low computational complexity and simple principles.

REFERENCES

[1] Venketeswaran, ABhishek, et al. "Recent advances in machine learning for fiber optic sensor applications." Advanced Intelligent Systems 4.1 (2022): 2100067.
[2] Floris, Ignazio, et al. "Fiber optic shape sensors: A comprehensive review." Optics and Lasers in Engineering 139 (2021): 106508.
[3] Lu, Yiang, et al. "Robust three-dimensional shape sensing for flexible endoscopic surgery using multi-core FBG sensors." IEEE Robotics and Automation Letters 6.3 (2021): 4835-4842.
[4] Liu, Yin, Ai Zhou, and Libo Yuan. "Multifunctional fiber-optic sensor, based on helix structure and fiber Bragg gratings, for shape sensing." Optics & Laser Technology 143 (2021): 107327.
[5] Lefloch, Damien, et al. "Comprehensive use of curvature for robust and accurate online surface reconstruction." IEEE transactions on pattern analysis and machine intelligence 39.12 (2017): 2349-2365.
[6] Le Tien, Mau, Khoi Nguyen Tan, and Romain Raffin. "Analysis of geometrical features of 3D model based on the surface curvature of a set of point cloud." Proceedings of the 5th International Conference on Future Networks and Distributed Systems. 2021.
[7] Ferraro, Davide, et al. "ImplantABle fiber Bragg grating sensor for continuous heart activity monitoring: ex-vivo and in-vivo validation." IEEE Sensors Journal 21.13 (2021): 14051-14059.
[8] Sefati, Shahriar, et al. "FBG-based large deflection shape sensing of a continuum manipulator: Manufacturing optimization." 2016 IEEE SENSORS. IEEE, 2016.
[9] Mohapatra, Ambarish G., et al. "IoT enABled distributed cardiac monitoring using Fiber Bragg Grating (FBG) sensing technology." Proceedings of the International Conference on Innovative Computing & Communication (ICICC). 2021.
[10] Ngiejungbwen, Looh Augustine, Hind Hamdaoui, and Ming-Yang Chen. "Polymer optical fiber and fiber Bragg grating sensors for biomedical engineering Applications: A comprehensive review." Optics & Laser Technology 170 (2024): 110187.
[11] Ramly, Ramzyzan, Wahyu Kuntjoro, and Mohd Kamil ABd Rahman. "Using embedded fiber Bragg grating (FBG) sensors in smart aircraft structure materials." Procedia Engineering 41 (2012): 600-606.
[12] Kent, Teresa A., et al. "Whisksight: A reconfigurABle, vision-based, optical whisker sensing array for simultaneous contact, airflow, and inertia stimulus detection." IEEE Robotics and Automation Letters 6.2 (2021): 3357-3364.
[13] Yang, Haokun, et al. "Whisker array based on fiber Bragg grating for surface shape sensing." 2021 International Conference on Optical Instruments and Technology: Optical Sensors and Applications. Vol. 12279. SPIE, 2022.
[14] Kent, Teresa A., et al. "Identifying Contact Distance Uncertainty in Whisker Sensing with Tapered, Flexible Whiskers." 2023 IEEE International Conference on Robotics and Automation (ICRA). IEEE, 2023.
[15] Liang, Wei, et al. "Highly sensitive fiber Bragg grating refractive index sensors." Applied physics letters 86.15 (2005).